scientific reports

Check for updates

OPEN

Foot trajectory as a key factor for diverse gait patterns in quadruped robot locomotion

Shura Suzuki[1,3]✉, Kosuke Matayoshi[2,3], Mitsuhiro Hayashibe[2] & Dai Owaki[2]✉

Four-legged robots are becoming increasingly pivotal in navigating challenging environments, such as construction sites and disaster zones. While substantial progress in robotic mobility has been achieved using reinforcement learning techniques, quadruped animals exhibit superior agility by employing fundamentally different strategies. Bio-inspired controllers have been developed to replicate and understand biological locomotion strategies. However, a comprehensive understanding of the influence of foot trajectories on gait patterns is still necessary. This study provides a groundbreaking perspective on the essential impact of these trajectory shapes on robotic gait patterns and overall performance. By employing the Unitree A1 robot model with a bio-inspired neural control system, our simulations demonstrate that specific trajectory shapes effectively replicate diverse and natural gait patterns, such as trotting, pacing, and galloping, thereby improving adaptability to diverse terrains. Specifically, trajectories designed for pacing exhibit superior performance on rough terrain, excelling in efficiency and adaptability over other gaits. This study highlights the significance of foot trajectory in augmenting robotic locomotion and establishes a new benchmark for developing advanced robots that operate effectively in unpredictable environments.

Keywords Foot trajectory, Quadruped gait, Intralimb coordination, Locomotion, Biomechanics, Decentralized control

Quadruped robots are emerging as a new means of mobility for navigating unstructured environments, such as construction sites and disaster zones[1–3]. Recent advancements in their mobility are largely attributed to motor control systems based on reinforcement learning techniques[4–11]. In contrast, quadruped animals exhibit remarkable agility through a fundamentally different control strategy, allowing them to walk shortly after birth and adapt to unexpected situations in real time[12]. Replicating such biological strategies contributes to the development of agile robots for use in the wild and provides valuable insights into animal motor control mechanisms.

Quadruped animals flexibly change their locomotion modes in response to varying conditions, including speed[13], terrain[14], and load[15]. This versatility in locomotion strategy contributes to their exceptional agility. These adaptive behaviors can be generated without cerebral control, as demonstrated by decerebrate animal experiments[12,16,17]. Instead, they rely on distributed control mechanisms within the spinal neural network, where central pattern generators (CPGs)[18,19] and local sensory feedback[20] play critical roles. Understanding the interplay between the CPGs and sensory feedback is essential for developing bio-inspired controllers that replicate the adaptability of animal locomotion.

Robotic studies have proposed bio-inspired controllers aimed at understanding and applying the principles of animal motor control[12]. These controllers often employ coupled-oscillator models, where individual oscillators represent CPGs and inter-oscillator couplings between them represent neural communication[21–27]. Additionally, integrating these models with sensory feedback mechanisms has successfully generated situation-dependent gaits[28–34]. Notwithstanding significant advances in bio-inspired models that incorporate CPGs for inter-leg coordination, current models have not effectively addressed intra-leg coordination, such as the coordination between the hip and knee joints, which significantly influences foot trajectory.

This study focuses on intra-leg coordination in quadruped robot locomotion and explores the effects of hip–knee joint coordination on the adaptability of robotic gait in complex terrains. Therefore, we developed a model using the Unitree A1 quadrupedal robot with a load-feedback-based inter-leg coordination model[31] of the CPG on the MuJoCo simulator[35] as a testbed for verification by focusing on two key parameters: the height and width

[1]Research Institute of Electrical Communication, Tohoku University, Sendai 980-8577, Japan. [2]Department of Robotics, Graduate School of Engineering, Tohoku University, Sendai 980-8579, Japan. [3]These authors contributed equally: Shura Suzuki and Kosuke Matayoshi. ✉email: shura.suzuki.c6@tohoku.ac.jp; owaki@tohoku.ac.jp

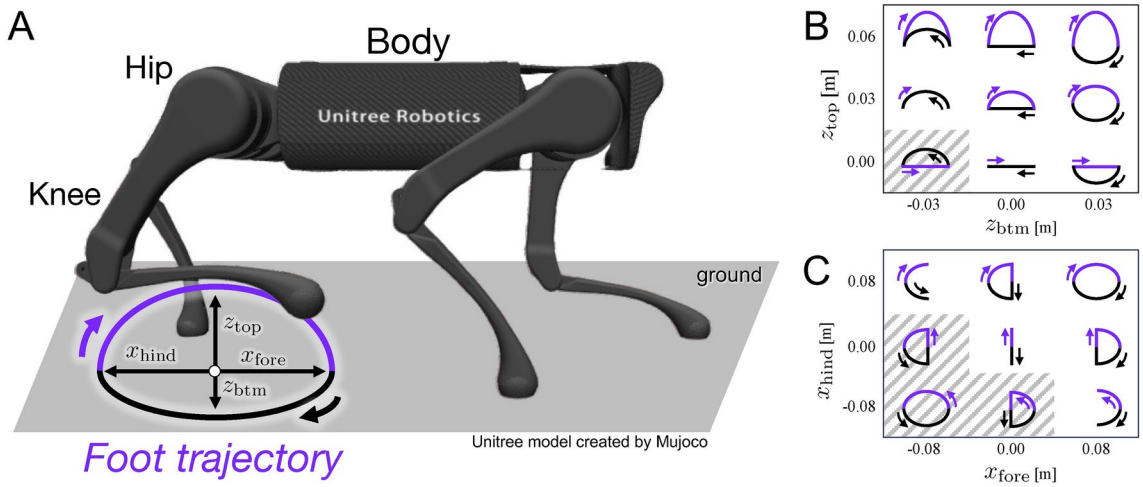

Fig. 1. Foot trajectory design based on oscillator phase. (**A**) Overview, (**B**) the variations in the trajectory height, (**C**) the variations in the trajectory width.

Robot length	0.50	[m]	Robot width	0.30	[m]
Robot height	0.37	[m]	Robot weight	12.453	[kg]
x_{off}	0.00	[m]	z_{off}	-2.9×10^{-1}	[m]
ω	10.0	[rad/s]	σ	0.131	[rad/Ns]

Table 1. Simulation parameters for trajectory height evaluation.

of the foot trajectory. Simulation experiments revealed that adjustments in foot trajectory height, influenced by hip–knee coordination, directly alter the resulting gait patterns, such as trot, pace, and gallop, which are crucial for effective locomotion on rough terrain. Our findings suggest that foot trajectory is a crucial parameter for generating gait patterns in response to environmental conditions. This underscores the significance of precise joint coordination for effective gait patterns. It also opens new avenues for applying these insights to practical robotic applications and biomechanical studies.

Results

We investigated how intra-leg coordination, especially the hip–knee relationship, affected the emergent gait and locomotion performance on flat and rough terrain. We adopted a foot trajectory using simple trigonometric equations and derived hip–knee coordination according to inverse kinematics:

$$\bar{x}_i = \begin{cases} x_{off} - x_{fore}\cos\phi_i & (\pi/2 < \phi_i \leq 3\pi/2) \\ x_{off} - x_{hind}\cos\phi_i & (-\pi/2 < \phi_i \leq \pi/2), \end{cases} \quad \bar{z}_i = \begin{cases} z_{off} + z_{ztop}\sin\phi_i & (0 < \phi_i \leq \pi) \\ z_{off} + z_{zbtm}\sin\phi_i & (\pi < \phi_i \leq 2\pi), \end{cases} \tag{1}$$

where $\bar{x}_i$ and $\bar{z}_i$ are the relative target positions from the shoulder/hip joint to the foot tip, respectively. These target positions draw an elliptical trajectory determined by the oscillator phase ϕ_i implemented on each leg. Index *i* denotes the leg number (left fore (LF), $i = 1$; right fore (RF), $i = 2$; left hind (LH), $i = 3$; and right hind (RH), $i = 4$). The variables x_{off} and z_{off} denote the offset positions; and x_{fore}, x_{hind}, z_{top}, and z_{btm} are the amplitudes of the target foot trajectory. By adjusting these amplitude parameters, the trajectory was modified in a simple and intuitive manner (Fig. 1).

First, we investigated various trajectory height parameter sets of z_{btm} and z_{top} on flat terrain because these are the main parameters for gait sustainability. Second, we investigated the effect of the trajectory width parameters x_{fore} and x_{hind} on three representative gaits. Finally, rough-terrain experiments were conducted, with three representative gait trajectories examined using flat-terrain experiments. Table 1 presents the remaining parameters. We determined the body size and weight based on those of an actual Unitree A1 robot. The control parameters were selected with physically plausible values based on body size and weight, with reference to our previous work[31]. The simulations lasted 100 s, and 100 experiments were conducted for each parameter set with randomized initial oscillator phases.

Trajectory height experiment

We investigated the relationship between the locomotion performance and trajectory height parameters, z_{btm} and z_{top}. These parameters determined the foot position height during the stance and swing phases (Fig. 1). We

examined z_{btm} from -0.03 to 0.03 m and z_{top} from 0.00 to 0.055 m to investigate various types of trajectories as shown in Fig. 1B, except for the parameter sets in $z_{\mathrm{top}} + z_{\mathrm{btm}} < 0$. This is because the trajectory involved an interchange between the upper and lower paths (diagonal stripes area in Fig. 1B). The trajectory width parameters x_{fore} and x_{hind} were 0.04 m. To evaluate the performance, we measured the locomotion sustainability, gait pattern, speed, and cost of transport (CoT), an energy efficiency metric, as shown in Fig. 2.

First, we investigated the locomotion sustainability, as shown in Fig. 2A. It analyzes the fall rate, which represents the proportion of falling accidents within 100 trials for each parameter set. Evidently, parameter combinations with higher z_{top} and z_{zbtm} values result in higher fall rates. Conversely, when z_{btm} had negative values, the robot demonstrated stable locomotion even with a higher z_{top}. Thus, a correlation exists between the trajectory and fall rate, which suggests a lower foot clearance with a higher sustainability. Additionally, we excluded parameter combinations with a high fall rate (> 50 %) from further analysis with other metrics and marked them with an 'x' (Fig. 2B–D).

The observed gait patterns are presented in Fig. 2B. This figure shows the observed phase relationships of the oscillators in each leg. The white points marked with bold lines indicate the parameters corresponding to the representative gait patterns depicted in Fig. 3A–C. Variations in the foot trajectory height gradually changed the phase relationship, revealing three distinct interlimb coordination patterns: trot, pace, and gallop. Trot, characterized by synchronized diagonal pairs of legs[36], is observed in the blue areas with lower z_{top} and positive z_{btm}. The pace, characterized by synchronized ipsilateral pairs of legs[36], is observed in the green areas with intermediate z_{top} and negative z_{btm}. The rotary gallop, featuring a rotational footfall pattern such as the left fore-left hind-right hind-right fore or vice versa[36], was observed in yellow-green areas with higher z_{top} and lower z_{btm}. Finally, although the parameter settings ($z_{\mathrm{btm}} = 0$ and $z_{\mathrm{top}} = 0$) represent a bound-like relationship representing red areas where contralateral pairs of legs synchronize, the legs struggle without lifting from the ground, and the robot model hardly moves (not shown in the results).

Figure 2C,D show the locomotion speed and CoT, respectively. The locomotion speed increased as z_{btm} decreased and z_{ztop} increased, whereas CoT maintained a relatively consistent value across a broader parameter range, encompassing a slower-to-faster parameter set. Locomotion speeds are related to gait patterns: trot corresponds to slower speeds (< 0.15 [m/s]), gallop corresponds to higher speeds (> 0.15 [m/s]), and pace corresponds to speeds over a wider range. In addition, the lowest CoT value for each gait was maintained within a certain range (CoT = 120–200). This result aligns with Hoyt and Taylor's horse experiment[13], in which gait changes in response to speed while maintaining a consistent CoT.

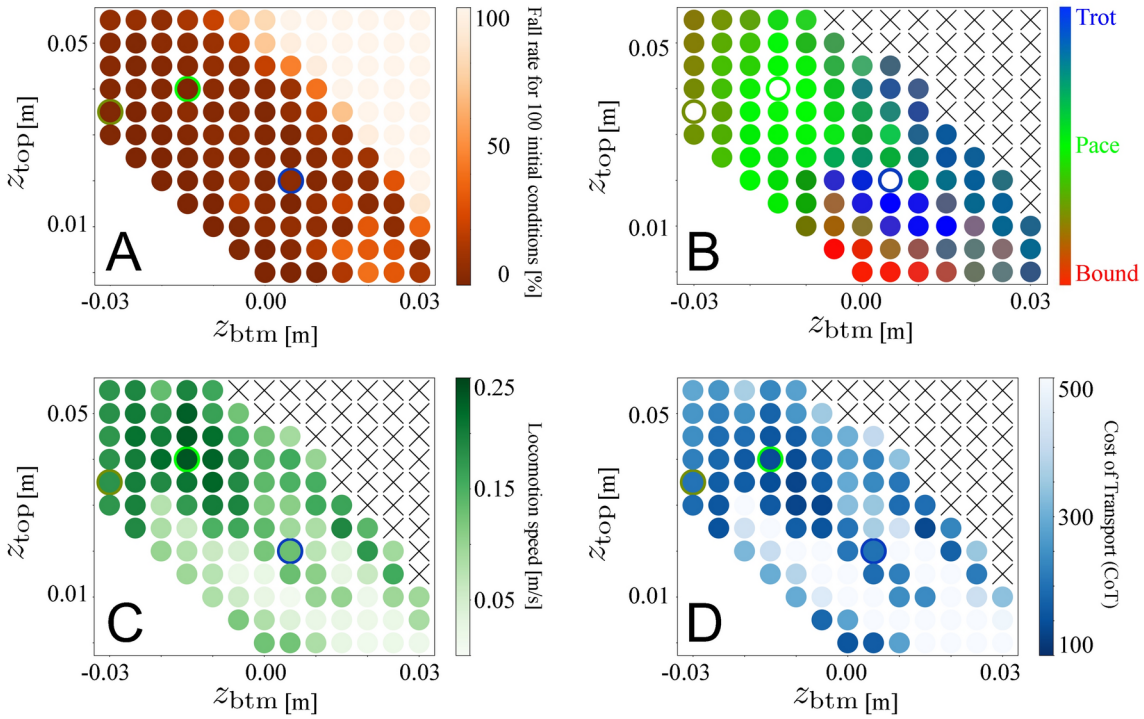

Fig. 2. Trajectory height experiment. (**A**) Fall rate for 100 initial conditions. We conducted 100 experiments over 100 s for each parameter set with randomized initial oscillator phases. (**B**) Gait distribution in parameter space $z_{\mathrm{btm}} - z_{\mathrm{top}}$ of foot trajectories. Visual colorization of gait patterns based on the phase relationship between oscillators (Fig. 6C). The points outlined with bold lines (blue, green, and dark green) indicate the parameters corresponding to Fig. 3A–C. (**C**) Locomotion speed: the green density indicates the magnitude of the locomotion speed. (**D**) CoT: the blue density indicates parameters with higher energy efficiency (lower CoT).

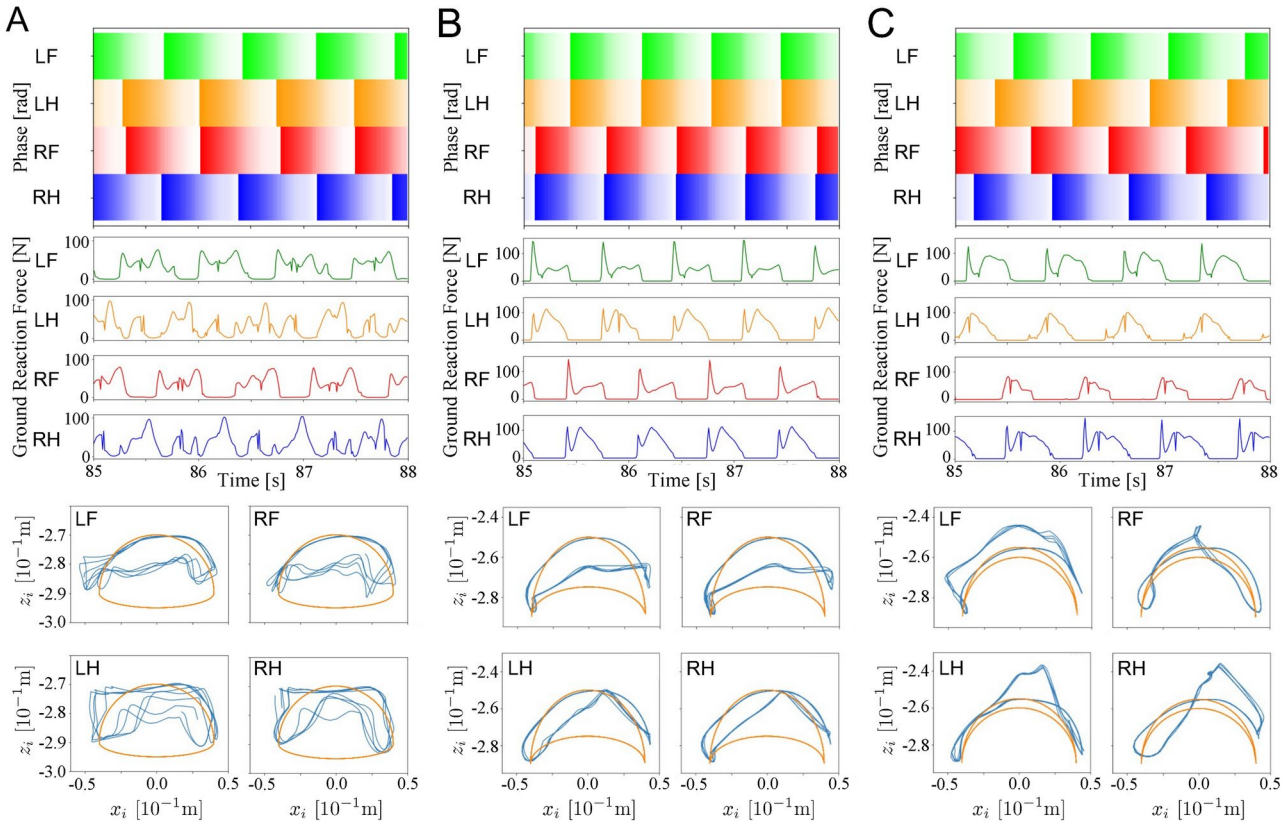

Fig. 3. Steady gait patterns: oscillator phases, GRFs, and target (orange) and generated (blue) foot trajectories. Trajectory parameters are (**A**) $z_{\mathrm{btm}} = 0.5 \times 10^{-2}$ m, $z_{\mathrm{top}} = 2.0 \times 10^{-2}$ m (**B**) $z_{\mathrm{btm}} = -1.5 \times 10^{-2}$ m, $z_{\mathrm{top}} = 4.0 \times 10^{-2}$ m and (**C**) $z_{\mathrm{btm}} = -3.0 \times 10^{-2}$ m, $z_{\mathrm{top}} = 3.5 \times 10^{-2}$ m.

Subsequently, we observed three gait patterns: trotting, pacing, and rotary galloping (see the accompanying video). Figure 3A–C illustrate the (top) time profiles of the oscillator phases, (center) ground reaction force (GRF), and (bottom) the target and generated foot trajectories for each gait pattern. The phase profiles were color-coded based on their values (color: $\phi_i = 0$, white: $\phi_i = 2\pi$). The target and generated trajectories are shown in orange and blue, respectively. Figure 3A illustrates synchronized diagonal pairs of legs, indicating a trot gait. The GRF profiles show that the robot drags its hind legs, which can cause slower movements. The target trajectory had a distorted elliptical shape ($z_{\mathrm{btm}} = 0.5 \times 10^{-2}$ m and $z_{\mathrm{top}} = 2.0 \times 10^{-2}$ m). The generated trajectory deviates from the target because of ground contact overload and the dragging of the legs.

Figure 3B shows that ipsilateral pairs of legs synchronize, indicating a paced gait. The target trajectory has a crescent-like shape with $z_{\mathrm{btm}} = -1.5 \times 10^{-2}$ m and $z_{\mathrm{top}} = 4.0 \times 10^{-2}$ m. The generated trajectory exhibits a stable and symmetrical bilateral pattern. The GRF profiles also showed bilateral symmetry, and the switching between the stance and swing phases was clear. These characteristics can be attributed to body swing. During the pace gait, the robot's posture changed in the roll direction, leading to ipsilateral synchronicity and ensuring sufficient ground clearance (see the accompanying video).

Figure 3C illustrates a footfall pattern characterized by a rotational sequence: LF-RF-RH-LH, indicating a rotary gallop gait. The parameters were $z_{\mathrm{btm}} = -3.0 \times 10^{-2}$ m and $z_{\mathrm{top}} = 3.5 \times 10^{-2}$ m. The target trajectory formed a sharper crescent-like shape with a lower z_{btm} than the pace gait ($z_{\mathrm{btm}} = -1.5 \times 10^{-2}$ m). The generated trajectory exhibited a stable pattern with bilateral asymmetry, in contrast to the paced gait. The GRF profiles also displayed asymmetry, with the leg that followed the ipsilateral leg (LF and RH) experiencing a higher GRF than the leg that followed the contralateral leg (LH and RF). This asymmetry can be attributed to the body swing. During the rotary gallop, the robot's posture changed in both the pitch and roll directions. When the stance leg switched to the ipsilateral leg (LF to LH), the posture changed in the pitch direction. Conversely, when the stance leg switched to the contralateral leg (LH to RH), the posture changed in the roll direction. Pitch-axis posture changes enhance the GRF values more than roll-axis posture changes, leading to GRF asymmetry.

Trajectory width experiment

We investigated the relationship between the locomotion performance and the trajectory width parameters, x_{fore} and x_{hind}, for the three representative gaits in Fig. 3 A–C. The parameters determine the anterior and posterior positions of the foot trajectory, respectively (Fig. 1). We examined x_{fore} and x_{hind} from -0.08 to 0.08 m, except for the parameter sets in $x_{\mathrm{fore}} + x_{\mathrm{hind}} < 0$, because the trajectory involved an interchange between the fore and hind paths (diagonal stripes area in Fig. 1C). The trajectory height parameters z_{btm} and z_{top}

are used for three gaits: trot ($z_{\mathrm{btm}} = 0.5 \times 10^{-2}$ m, $z_{\mathrm{top}} = 2.0 \times 10^{-2}$ m), pace ($z_{\mathrm{btm}} = -1.5 \times 10^{-2}$ m, $z_{\mathrm{top}} = 4.0 \times 10^{-2}$ m), gallop ($z_{\mathrm{top}} = 3.5 \times 10^{-2}$ m), as shown in Fig. 3. Figure 4 shows the phase relationship, speed, and CoT for each condition. The conditions with a high fall rate (> 50 %) are marked with an 'x.'

Figure 4A–C show the results for the parameter sets $z_{\mathrm{btm}} = 0.5 \times 10^{-2}$ m and $z_{\mathrm{top}} = 2.0 \times 10^{-2}$ m. A high x_{fore} tends to have higher fall rates, and combinations of higher x_{fore} and x_{hind} are likely to increase speed and energy efficiency. Thus, a wider stride yields a higher speed, but an excessive stride length leads to instability. This feature is consistent with the other parameters for the pace gait (Fig. 4E) and the gallop gait (Fig. 4H), although the parameter set showing the highest speed/energy efficiency is different in response to the emerging gait. The emerged gait varies according to the trajectory width parameters (Fig. 4A), where positive x_{fore} and x_{hind} indicate the blue area, indicating trot, and negative x_{fore} or x_{hind} indicate the green area, indicating pace. However, because the parameter sets in the green area hardly moved, variations in the trajectory width parameters did not generate various gait patterns. This tendency was similar to that of the others, as shown in Fig. 4. Therefore, although the trajectory height parameters seemed to be determinants of the emerged gait, the trajectory width parameters had little correlation with the gait in the experiments.

Rough terrain experiment

We investigated locomotion performance on rough terrain. The rough terrain consists of blocks of various heights (Fig. 5A) inspired by[37]. The height of each block was randomly assigned with a uniform distribution. We designed the maximum block height (0.0–0.5 m) and block area (0.04×0.04-0.48×0.48 m^2). We constructed 100 rough terrains for each condition and conducted walking simulations using three representative foot trajectories, as shown in Fig. 3. The travel distance during each trial was measured as a performance metric. The raincloud plots in Fig. 5 show that the travel distance of each foot trajectory parameter is (D) $z_{\mathrm{btm}} = 0.5 \times 10^{-2}$ m, $z_{\mathrm{top}} = 2.0 \times 10^{-2}$ m, (E) $z_{\mathrm{btm}} = -1.5 \times 10^{-2}$ m, $z_{\mathrm{top}} = 4.0 \times 10^{-2}$ m, and (F) $z_{\mathrm{btm}} = -3.0 \times 10^{-2}$ m, $z_{\mathrm{top}} = 3.5 \times 10^{-2}$ m.

The common tendency is that the higher the maximum block height, the shorter the travel distance, and the larger the block area, the longer the travel distance, which aligns intuitively. When the maximum height was 0.05 m, the robot hardly navigated regardless of the foot trajectory. With the foot trajectory for the trot gait (Fig. 5D), the robot barely navigated even slight irregularities, with a maximum height of 0.01 m. With the foot trajectory for the pace gait (Fig. 5E), when the maximum height is 0.01 m, the robot can navigate the rough terrain and move 10 m, approximately 80 % of the distance compared to that of the flat terrain experiment,

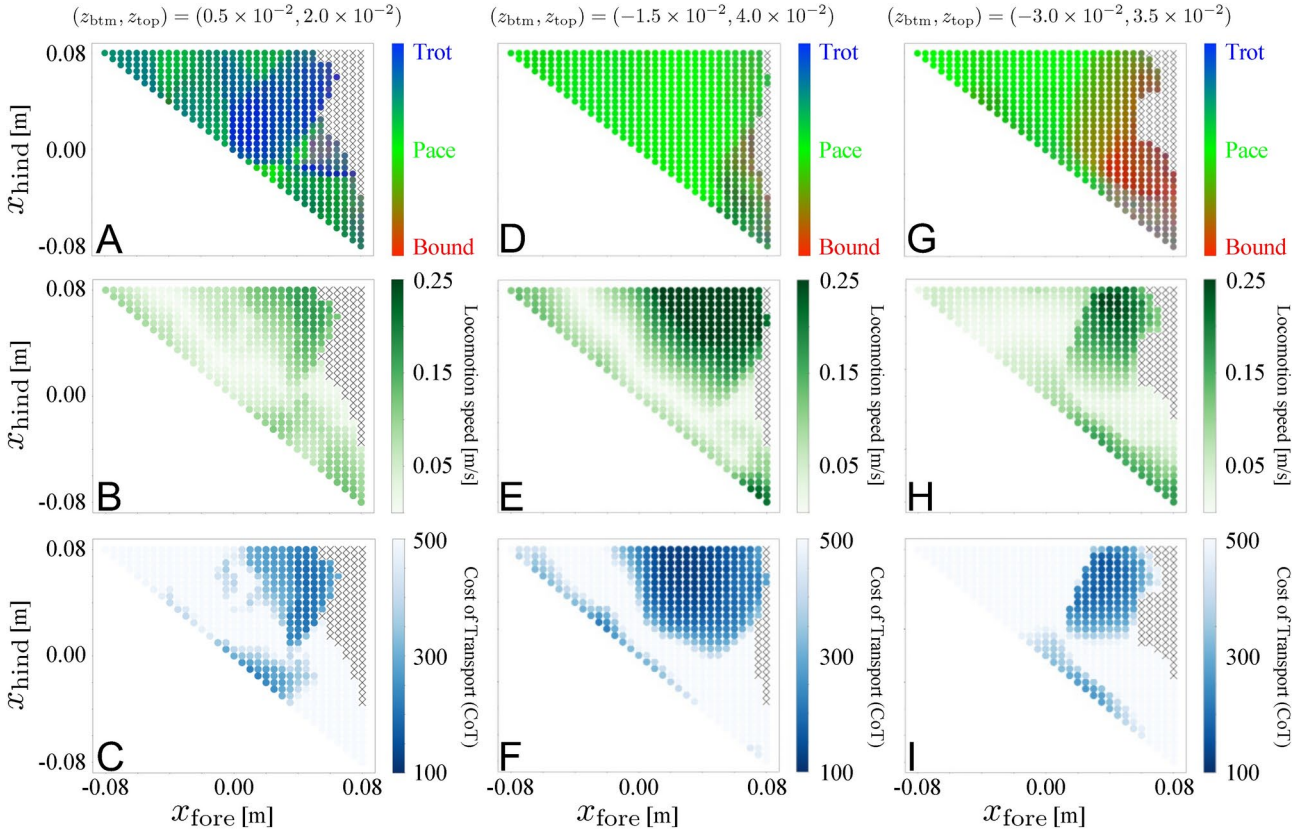

Fig. 4. Trajectory width experiment. Gait distribution, locomotion speed and CoT, (**A**)–(C) for $z_{\mathrm{btm}} = 0.5 \times 10^{-2}$ m, $z_{\mathrm{top}} = 2.0 \times 10^{-2}$ m as shown in Fig. 3A, (**D**)–(**F**) for $z_{\mathrm{btm}} = -1.5 \times 10^{-2}$ m, $z_{\mathrm{top}} = 4.0 \times 10^{-2}$ m as shown in Fig. 3B, (**G**)–(**I**) for $z_{\mathrm{btm}} = -3.0 \times 10^{-2}$ m, $z_{\mathrm{top}} = 3.5 \times 10^{-2}$ m as shown in Fig. 3C, respectively.

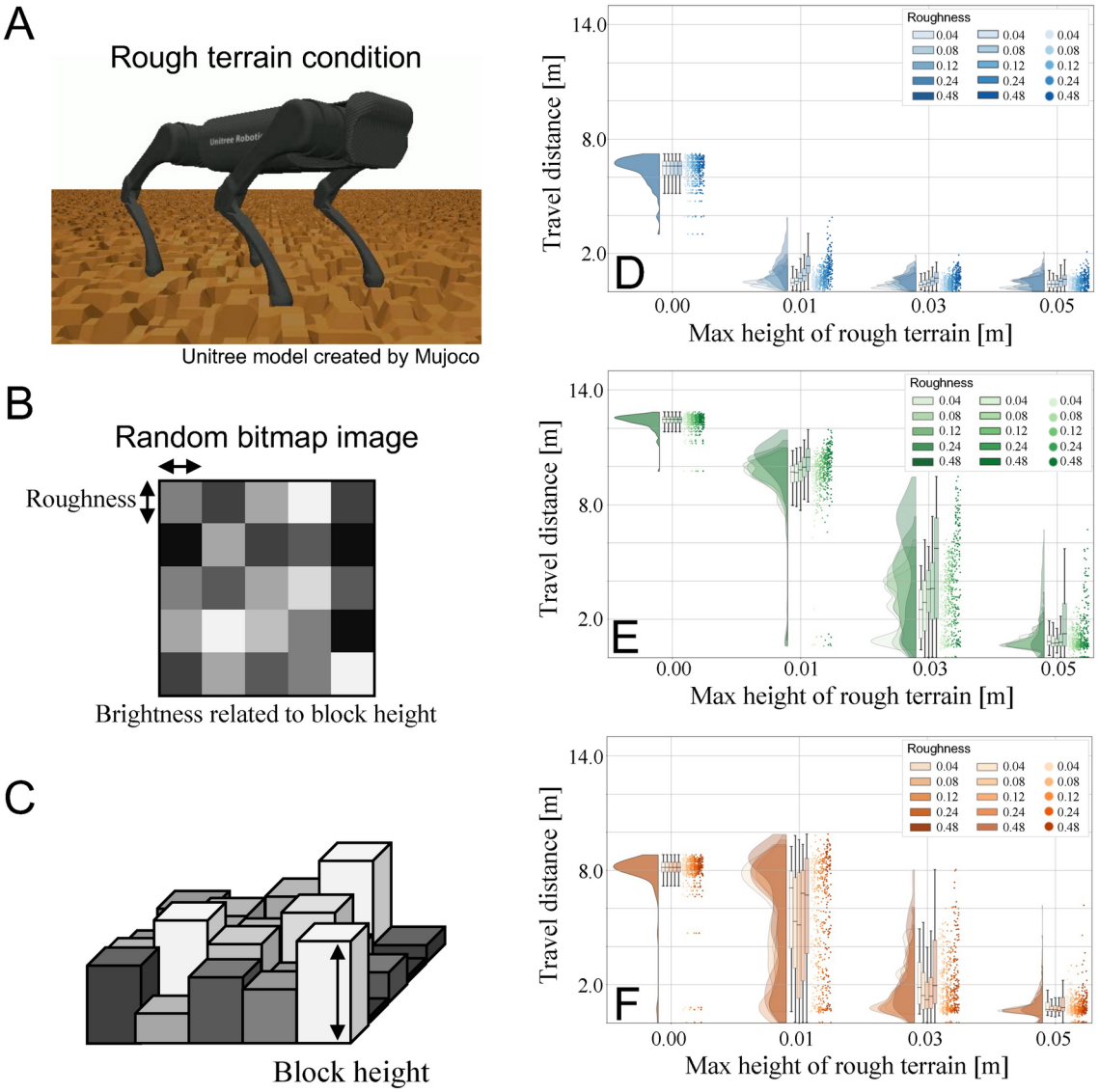

Fig. 5. Rough terrain experiment: (**A**) rough terrain consisting of variable height blocks generated by (**B**) a random bitmap image in which pixel size determines the block area and pixel brightness determines the block height (**C**). Travel distance on rough terrain experiment with foot trajectory parameters of (**D**) $z_{\mathrm{btm}} = 0.5 \times 10^{-2}$ m, $z_{\mathrm{top}} = 2.0 \times 10^{-2}$ m, (**E**) $z_{\mathrm{btm}} = -1.5 \times 10^{-2}$ m, $z_{\mathrm{top}} = 4.0 \times 10^{-2}$ m, (**F**) $z_{\mathrm{btm}} = -3.0 \times 10^{-2}$ m, $z_{\mathrm{top}} = 3.5 \times 10^{-2}$ m.

with a few exceptions. When the maximum height was 0.03 m, there was a larger variance in the travel distance, and some trials achieved 8 m, which is approximately 65 % of the distance compared to that of the flat terrain experiment. From the foot trajectory of the gallop gait (Fig. 5F), when the maximum height was 0.01 m, the travel distance had a larger variance, and some trials achieved a longer travel distance than the flat terrain experiment. When the maximum height was 0.03 m, many cases were less than 2 m, and the travel distance was likely to be shorter than that of the parameters, as shown in Fig. 5E.

Discussion

This study demonstrated that a sensory-feedback-based inter-leg coordination mechanism can reproduce diverse gait patterns by changing intra-leg coordination, that is, the foot trajectory (Fig. 1). The significance lies in presenting adaptive integration between inter- and intra-leg coordination for gait generation mechanisms. The conventional approach to gait generation mechanisms relies on the coupling of neural circuit CPGs[21,23,28,32,38,39], which encounters the challenge of spontaneously modulating gait patterns in response to variables such as speed and environment, even with intra-leg coordination. Shafiee et al.[34] adopted an integrated approach for CPG-based control and deep reinforcement learning. This study focused on terrain properties as a factor in gait transitions and reproduced walk-trot and trot-pronk gait transitions. The results were successful in gait transitions, including intra-leg coordination, in response to situations. However, inter-leg coordination is strictly

determined by neural couplings between CPGs, and the study did not discuss the relationship between inter- and intra-leg coordination for gait generation. Nyakatura et al.[40] reproduced extinct animal gait patterns by optimizing inter- and intra-leg coordination using fossil footprints as constraints. However, the correlation between inter-joint coordination and the resulting gait patterns has not been discussed clearly. Conversely, as behavioral evidence of animals, Catavitello et al.[41] reported a correlation between dog gaits and vertical and anteroposterior changes in the foot trajectory in the sagittal plane. This correlation was consistent with our simulation results (Fig. 2). These findings suggest that inter-joint coordination within a leg, previously overlooked, is crucial in generating diverse gait patterns that depend on inter-leg coordination.

Speed-related gait transitions occur in many quadruped animals; however, the factors that trigger gait changes remain unclear[42]. Alexander presented a correlation between the gait patterns and the *Froude number*[43]. Hoyt and Taylor suggested that horses change their gait patterns in response to the locomotion speed to reduce energy expenditure (oxygen consumption)[13]. A similar tendency has been observed in other quadruped animals[42]. Farley and Taylor stated that the trot-gallop gait transition in horses is triggered by reaching a peak ground reaction force at a critical level[15]. Schöner et al. stated that gait transition is a phase transition phenomenon in a nonequilibrium system between attractors[44]. Granatosky et al.[42] suggested that reducing instability while maintaining locomotion rhythms triggered a gait transition. Shafiee et al.[34] stated that gait transition could be triggered by environmental perception to avoid falling into challenging terrain. The results in Fig. 2 show that gait changes result from modulating the foot trajectory height. However, foot trajectory width does not have a significant impact on gait changes compared to locomotion performance. These facts suggest that situation-dependent intra-leg coordination adjusts the foot trajectory, resulting in gait transition. Although our study does not propose a novel hypothesis for gait transition mechanisms, it highlights the importance of foot trajectory as a key factor in gait transition.

The limitations and future directions of this study are as follows: First, the foot trajectory was predefined. Although we observed adaptive inter-leg coordination to some extent, adaptation to dynamically changing environments remained highly challenging. Investigating adaptive intra-leg coordination mechanisms using reinforcement learning methods[45], *Tegotae*-based control[46] with local sensor feedback, or their combination[47] could further enhance quadruped gait performance. Second, we need to further investigate foot trajectory parameters. While the study examined the impact of trajectory height and width separately, it did not explore the synergetic effects of these parameters (we have presented our preliminary validation for these synergetic effects in Supplementary Materials). The role of trajectory parameters related to the left-right direction, which is linked to turning and balancing, also remains unclear. Investigating the combinations of these parameters will aid in understanding their synergetic effects. To examine the intra-leg coordination with multi-degrees of freedom, the forward kinematics approach is useful, in contrast to using the target trajectory with the inverse kinematics approach. Figure 3 shows that the generated trajectory deviates from the target trajectory. These discrepancies could be due to the relatively small value of the PD control gain for the effective generation of robot-environment interaction; hence, we can mitigate them by increasing the gains, but this would also influence emergent gait with a load-dependent feedback mechanism and it needs further investigation. Finally, the real-world validation of the control mechanism is a topic for future work. These attempts will provide insights into the relationship between gait patterns and locomotion performance and enhance our understanding of gait transition mechanisms in animals.

Methods

Quadruped robot model

We adopted the Unitree A1 (Unitree) as the quadruped robot model, as shown in Fig. 6A. This robot model has 12 degrees of freedom (DoFs). Each leg consists of three DoFs. Two DoFs were present in the pitch and roll axes of the shoulder and hip joints, and one DoF was present in the pitch axis of the elbow and knee joints. Force sensors were installed on the tip of each foot. The physics simulator MuJoCo[35] is used in the simulation experiment. The collision model implemented in MuJoCo is highly accurate and can model the contact and repulsive forces between objects with complex shapes while considering their shape, size, and material properties. This algorithm allows for a precise simulation of the contact and reaction forces.

CPG-based controller

Each leg has a phase oscillator, representing CPG, and the oscillator phase determines the target foot trajectory, as described in Equation 1. Based on the target foot trajectory, the target angles of the robot joints (Fig. 6B) were calculated according to inverse kinematics, as described in[24]. The leg actuators achieved the target angles using proportional derivative (PD) control.

The time evolution of the oscillator phase is derived using the following differential equation:

$$\dot{\phi}_i = \omega - \sigma N_i \cos\phi_i, \tag{2}$$

where ω is the intrinsic angular frequency of the oscillator, σ is the feedback gain, and N_i is the ground reaction force (GRF) detected by the foot sensor. The feedback modifies the phase toward $3\pi/2$ when the leg obtains GRF ($N_i > 0$), which helps maintain the target position in the stance phase and keeps the leg on the ground (Fig. 6C). The GRF information is the outcome of the intricate interplay between the robot and the environment and is reflected in the motion state of the other legs. Therefore, GRF feedback helps establish self-organized interlimb coordination without information from the other legs. It also realizes speed-dependent gait transitions similar to those observed in quadrupeds[30,31].

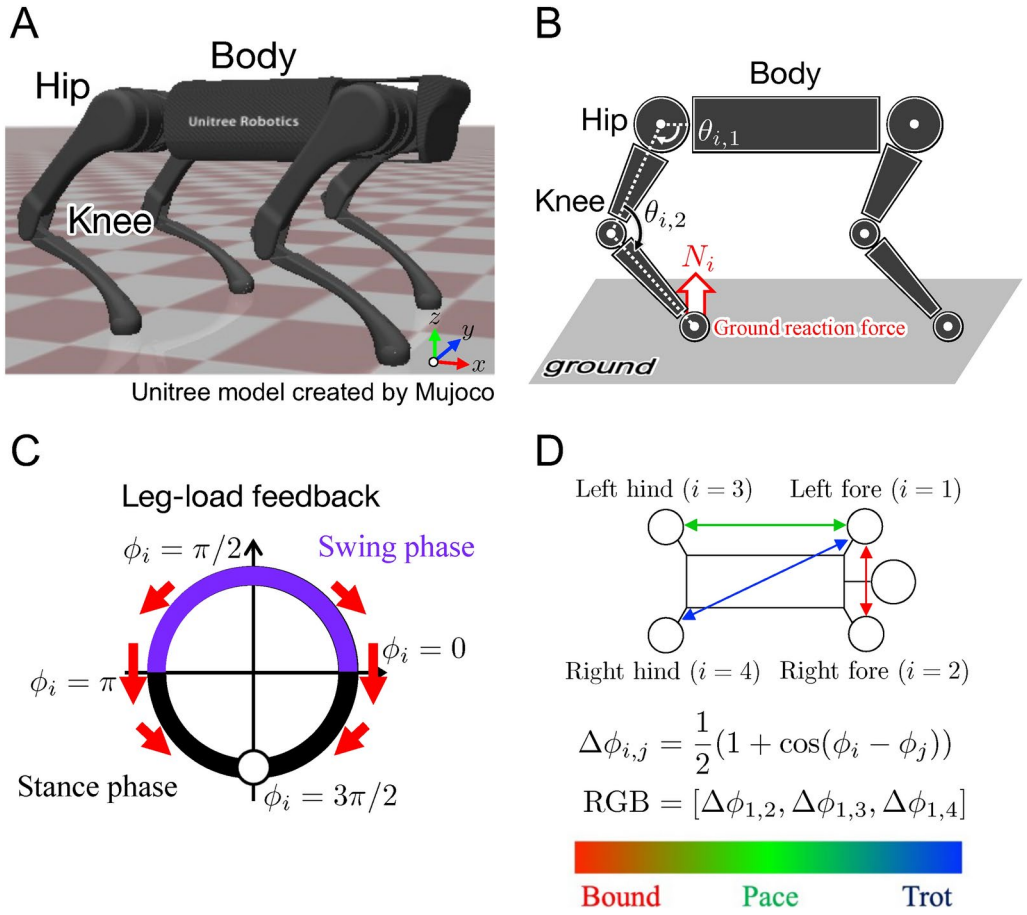

Fig. 6. Quadruped robot model (Unitree A1). (**A**) Overview. (**B**) Leg kinematics. (**C**) Effect of local sensory feedback on each phase oscillator. (**D**) Gait visual colorization based on the phase differences of oscillators.

Gait classification

For gait classification, we focused on interlimb coordination and used the phase relationship $\Delta\phi_{i,j}$ between the oscillators.

$$\Delta\phi_{i,j} = \frac{1}{2}(1 + \cos(\phi_i - \phi_j)) \tag{3}$$

where $\Delta\phi_{i,j}$ is the phase relationship between the *i*th and *j*th oscillators. The value of $\Delta\phi_{i,j}$ ranges from 0 to 1, with 1 indicating the in-phase and 0 indicating anti-phase of the oscillators. Here, we evaluate the resulting gait using the phase relationship between the left foreleg and the other legs $[\Delta\phi_{1,2}, \Delta\phi_{1,3}, \Delta\phi_{1,4}]$ and an RGB color model (Fig. 6D).

Evaluation indexes

We used three evaluation indexes: fall rate, locomotion speed, and CoT. The fall rate is the ratio of trials in which falls of the robot were detected. A fall is assessed when the height of the center of mass (CoM) is lower than a specified threshold. The locomotion speed was measured using the distance traveled within a certain duration. The CoT is an energy efficiency index described by the following equation[48]:

$$\begin{aligned} \mathrm{CoT} &= \frac{\Sigma_{i,j} e_{i,j}}{MgD}, \\ e_{i,j} &= \int_{T}^{T'} \left(\delta(\dot{\theta}_{i,j}(t)\tau_{i,j}(t)) + \gamma\tau_{i,j}^2(t)\right) \mathrm{d}t, \\ \delta(x) &= \max[0, x], \end{aligned} \tag{4}$$

where $\dot{\theta}_{i,j}$ is the angular velocity of the joint, $\tau_{i,j}$ is the input torque of the joint, and the index *j* denotes the joint number (hip:$j = 1$, knee:$j = 2$). The evaluation begins at T and ends at T'. A constant value γ (set to 0.005)

determines the maximum efficiency of the actuator[48], M is the total robot weight, and D is the distance traveled during the evaluation period.

Rough terrain setup

We used rough terrain with blocks of various heights generated by random bitmap images, as shown in Fig. 5B. Each pixel corresponds to a block, and the brightness is the block height, with white being the highest and black the lowest. We prepared 100 random bitmap images and assigned the parameters of the block area and maximum block height to each image to generate a simulated environment (Fig. 5C).

Data availability

The original contributions presented in the study are included in the article/Supplementary Material, further inquiries can be directed to the corresponding author.

Received: 7 June 2024; Accepted: 19 December 2024
Published online: 13 January 2025

References

1. Hoeller, D., Rudin, N., Sako, D. & Hutter, M. Anymal parkour: Learning agile navigation for quadrupedal robots. *Sci. Robot.* **9**, eadi7566 (2024).
2. Spot—The Agile Mobile Robot,. https://bostondynamics.com/products/spot/. Accessed on May 15th, 2024.
3. A1—Highly Integrated, Pushing limits—Unitree. https://www.unitree.com/a1/. Accessed on May 15th, 2024.
4. Hwangbo, J. *et al.* Learning agile and dynamic motor skills for legged robots. *Sci. Robot.* **4** (2019).
5. Bellicoso, D., Jenelten, F., Gehring, C. & Hutter, M. Dynamic locomotion through online nonlinear motion optimization for quadrupedal robots. *IEEE Robot. Autom. Lett.* **3**, 2261–2268 (2018).
6. Bellegarda, G., Chen, Y., Liu, Z. & Nguyen, Q. Robust high-speed running for quadruped robots via deep reinforcement learning. In *2022 IEEE/RSJ International Conference on Intelligent Robots and Systems (IROS)*, 10364–10370. https://doi.org/10.1109/IROS47612.2022.9982132 (2022).
7. Lee, J., Hwangbo, J., Wellhausen, L., Koltun, V. & Hutter, M. Learning quadrupedal locomotion over challenging terrain. *Sci. Robot.* **5** (2020).
8. Aractingi, M. et al. Controlling the solo12 quadruped robot with deep reinforcement learning. *Sci. Rep.* **13**, 11945 (2023).
9. Ji, Q. et al. Synthesizing the optimal gait of a quadruped robot with soft actuators using deep reinforcement learning. *Robot. Comput. Integrated Manufact.* **78**, 102382 (2022).
10. Tan, J. *et al.* Sim-to-real: Learning agile locomotion for quadruped robots. CoRR arXiv:1804.10332 (2018).
11. Jain, D., Iscen, A. & Caluwaerts, K. Hierarchical reinforcement learning for quadruped locomotion. In *2019 IEEE/RSJ International Conference on Intelligent Robots and Systems (IROS)*, 7551–7557. https://doi.org/10.1109/IROS40897.2019.8967913 (2019).
12. Ijspeert, A. J. & Daley, M. A. Integration of feedforward and feedback control in the neuromechanics of vertebrate locomotion: a review of experimental, simulation and robotic studies. *J. Exp. Biol.* **226**, jeb245784 (2023).
13. Hoyt, D. F. & Taylor, C. Gait and the energetics of locomotion in horses. *Nature* **292**, 239–240 (1981).
14. Frigon, A. et al. Split-belt walking alters the relationship between locomotor phases and cycle duration across speeds in intact and chronic spinalized adult cats. *J. Neurosci.* **33**, 8559–8566 (2013).
15. Farley, C. & Taylor, C. A mechanical trigger for the trot-gallop transition in horses. *Science* **253**(5017), 306–308 (1991).
16. Grillner, S. & El Manira, A. Current principles of motor control, with special reference to vertebrate locomotion. *Physiol. Rev.* (2019).
17. Leiras, R., Cregg, J. M. & Kiehn, O. Brainstem circuits for locomotion. *Annu. Rev. Neurosci.* **45**, 63–85 (2022).
18. Kiehn, O. Locomotor circuits in the mammalian spinal cord. *Annu. Rev. Neurosci.* **29**, 279–306 (2006).
19. Kiehn, O. Decoding the organization of spinal circuits that control locomotion. *Nat. Rev. Neurosci.* **17**, 224–238 (2016).
20. Rossignol, S., Dubuc, R. & Gossard, J. Dynamic sensorimotor interactions in locomotion. *Physiol. Rev.* **86**(1), 89–154 (2006).
21. Righetti, L. & Ijspeert, A. J. Pattern generators with sensory feedback for the control of quadruped locomotion. In *2008 IEEE International Conference on Robotics and Automation*, 819–824 (2008).
22. Spröwitz, A. et al. Towards dynamic trot gait locomotion: Design, control, and experiments with cheetah-cub, a compliant quadruped robot. *Int. J. Robot. Res.* **32**, 932–950 (2013).
23. Ajallooeian, M., Gay, S., Tuleu, A., Spröwitz, A. & Ijspeert, A. J. Modular control of limit cycle locomotion over unperceived rough terrain. *2013 IEEE/RSJ International Conference on Intelligent Robots and Systems*, 3390–3397 (2013).
24. Bellegarda, G. & Ijspeert, A. J. CPG-RL: Learning central pattern generators for quadruped locomotion. *IEEE Robot. Autom. Lett.* **7**, 12547–12554 (2022).
25. Shao, Y. et al. Learning free gait transition for quadruped robots via phase-guided controller. *IEEE Robot. Autom. Lett.* **7**, 1230–1237 (2022).
26. Ruppert, F. & Badri-Spröwitz, A. Learning plastic matching of robot dynamics in closed-loop central pattern generators. *Nat. Mach. Intell.* **4**, 652–660 (2022).
27. Mo, A., Izzi, F., Gönen, E. C., Haeufle, D. & Badri-Spröwitz, A. Slack-based tunable damping leads to a trade-off between robustness and efficiency in legged locomotion. *Sci. Rep.* **13**, 3290 (2023).
28. Kimura, H., Akiyama, S. & Sakurama, K. Realization of dynamic walking and running of the quadruped using neural oscillator. *Auton. Robot.* **7**, 247–258 (1999).
29. Fukuoka, Y., Habu, Y. & Fukui, T. A simple rule for quadrupedal gait generation determined by leg loading feedback: a modeling study. *Sci. Rep.* **5** (2015).
30. Owaki, D., Kano, T., Nagasawa, K., Tero, A. & Ishiguro, A. Simple robot suggests physical interlimb communication is essential for quadruped walking. *J. R. Soc. Interface* **10** (2013).
31. Owaki, D. & Ishiguro, A. A quadruped robot exhibiting spontaneous gait transitions from walking to trotting to galloping. *Sci. Rep.* **7** (2017).
32. Fukuhara, A., Owaki, D., Kano, T., Kobayashi, R. & Ishiguro, A. Spontaneous gait transition to high-speed galloping by reconciliation between body support and propulsion. *Adv. Robot.* **32**, 794–808 (2018).
33. Fukui, T., Matsukawa, S., Habu, Y. & Fukuoka, Y. Gait transition from pacing by a quadrupedal simulated model and robot with phase modulation by vestibular feedback. *Robotics* **11**, 3 (2021).
34. Shafiee, M., Bellegarda, G. & Ijspeert, A. Viability leads to the emergence of gait transitions in learning agile quadrupedal locomotion on challenging terrains. *Nat. Commun.* **15**, 3073 (2024).

35. Todorov, E., Erez, T. & Tassa, Y. Mujoco: A physics engine for model-based control. In *2012 IEEE/RSJ International Conference on Intelligent Robots and Systems*, 5026–5033 (2012).
36. Hildebrand, M. The quadrupedal gaits of vertebrates. *Bioscience* **39**, 766 (1989).
37. Sponberg, S. & Full, R. Neuromechanical response of musculo-skeletal structures in cockroaches during rapid running on rough terrain. *J. Exp. Biol.* **211**, 433–446 (2008).
38. Danner, S. M., Wilshin, S. D., Shevtsova, N. A. & Rybak, I. A. Central control of interlimb coordination and speed-dependent gait expression in quadrupeds. *J. Physiol.* **594**, 6947–6967 (2016).
39. Molkov, Y. I. *et al.* Sensory feedback and central neuronal interactions in mouse locomotion. *bioRxiv* (2023).
40. Nyakatura, J. A. et al. Reverse-engineering the locomotion of a stem amniote. *Nature* **565**, 351–355 (2019).
41. Catavitello, G., Ivanenko, Y. P. & Lacquaniti, F. Planar covariation of hindlimb and forelimb elevation angles during terrestrial and aquatic locomotion of dogs. *PLoS ONE* **10** (2015).
42. Granatosky, M. C. et al. Inter-stride variability triggers gait transitions in mammals and birds. *Proc. R. Soc. B* **285**, 20181766 (2018).
43. Alexander, R. M. Optimization and gaits in the locomotion of vertebrates. *Physiol. Rev.* **69**, 1199–1227 (1989).
44. Schöner, G., Jiang, W. & Kelso, J. A. S. A synergetic theory of quadrupedal gaits and gait transitions. *J. Theor. Biol.* **142**(3), 359–391 (1990).
45. Sutton, R. S. & Barto, A. G. *Reinforcement Learning: An Introduction* 2nd edn. (The MIT Press, 2018).
46. Owaki, D., Goda, M., Miyazawa, S. & Ishiguro, A. A minimal model describing hexapedal interlimb coordination: The tegotae-based approach. *Front. Neurorobot.* **11** (2017).
47. Herneth, C., Hayashibe, M. & Owaki, D. Learnable tegotae-based feedback in cpgs with sparse observation produces efficient and adaptive locomotion. In *2023 IEEE International Conference on Robotics and Automation (ICRA)*, 1155–1161 (2023).
48. Nishii, J. Legged insects select the optimal locomotor pattern based on the energetic cost. *Biol. Cybern.* **83**, 435–442 (2000).

Acknowledgements

This study was supported by JSPS KAKENHI Grant Numbers JP23H00481 and JP22KJ2098.

Author contributions

M.H. and D.O. designed the study. S.S. and D.O. conceived the experiments. S.S., K.M., and D.O. designed the robot model. K.M. conducted the experiments. S.S. and D.O. analyzed the results. All authors reviewed the manuscript.

Declarations

Competing interests

The authors declare no competing interests.

Additional information

Supplementary Information The online version contains supplementary material available at https://doi.org/10.1038/s41598-024-84060-5.

Correspondence and requests for materials should be addressed to S.S. or D.O.

Reprints and permissions information is available at www.nature.com/reprints.

Publisher's note Springer Nature remains neutral with regard to jurisdictional claims in published maps and institutional affiliations.